Acta Crystallographica Section D
Biological Crystallography
ISSN 1399-0047

Coiled-coil deformations in crystal structures: the *measles virus* phosphoprotein multimerization domain as an illustrative example

David Blocquel,[a,b]‡ Johnny Habchi,[a,b]‡ Eric Durand,[a,b] Marion Sevajol,[a,b] François Ferron,[a,b] Jenny Erales,[a,b] Nicolas Papageorgiou[a,b]* and Sonia Longhi[a,b]*

[a]Aix-Marseille University, AFMB UMR 7257, 13288 Marseille, France, and [b]CNRS, AFMB UMR 7257, 13288 Marseille, France

‡ These authors contributed equally to the work.

Correspondence e-mail: nicolas.papageorgiou@afmb.univ-mrs.fr, sonia.longhi@afmb.univ-mrs.fr

Received 9 January 2014
Accepted 31 January 2014

PDB references: *measles virus* phosphoprotein multimerization domain, 4bhv; 4c5q

The structures of two constructs of the *measles virus* (MeV) phosphoprotein (P) multimerization domain (PMD) are reported and are compared with a third structure published recently by another group [Communie *et al.* (2013), *J. Virol.* **87**, 7166–7169]. Although the three structures all have a tetrameric and parallel coiled-coil arrangement, structural comparison unveiled considerable differences in the quaternary structure and unveiled that the three structures suffer from significant structural deformation induced by intermolecular interactions within the crystal. These results show that crystal packing can bias conclusions about function and mechanism based on analysis of a single crystal structure, and they challenge to some extent the assumption according to which coiled-coil structures can be reliably predicted from the amino-acid sequence. Structural comparison also highlighted significant differences in the extent of disorder in the C-terminal region of each monomer. The differential flexibility of the C-terminal region is also supported by size-exclusion chromatography and small-angle X-ray scattering studies, which showed that MeV PMD exists in solution as a dynamic equilibrium between two tetramers of different compaction. Finally, the possible functional implications of the flexibility of the C-terminal region of PMD are discussed.

1. Introduction

Measles virus (MeV) is a member of the *Paramyxoviridae* family. Its non-segmented, single-stranded, negative-sense RNA genome is encapsidated by monomers of the nucleoprotein (N) within a helical nucleocapsid. This ribonucleoproteic complex is the template for both transcription and replication. The viral RNA-dependent RNA polymerase (L) is tethered onto the nucleocapsid template *via* the viral phosphoprotein (P), which is therefore an essential polymerase cofactor.

Beyond its role in recruiting the L protein, P also serves as a chaperone for N: by binding to the monomeric form of N (referred to as N^o) it prevents illegitimate self-assembly of the latter (Huber *et al.*, 1991; Spehner *et al.*, 1997), thereby leading to formation of the N^o–P complex, which is used for the encapsidation of the nascent genomic RNA chain during replication (for reviews, see Lamb & Parks, 2007; Albertini *et al.*, 2005; Roux, 2005; Blocquel *et al.*, 2012).

In previous studies, using both computational and experimental approaches, we have shown that both MeV N and P proteins possess long intrinsically disordered domains (Karlin, Longhi & Canard, 2002; Longhi *et al.*, 2003; Bourhis *et al.*,

2004). The P protein contains a long N-terminal disordered region (PNT; amino acids 1–230; Karlin, Longhi, Receveur *et al.*, 2002) and a C-terminal moiety (PCT; amino acids 231–507). PCT has a modular organization, being composed of alternating disordered and ordered regions: it embraces a predicted disordered region (amino acids 231–303) referred to as the spacer, a structured region (amino acids 304–375) referred to as the PMD (P multimerization domain), a disordered linker (amino acids 377–458) and a globular region (amino acids 459–507) referred to as the X domain (XD) (Fig. 1; Karlin *et al.*, 2003). The structure of the XD has been solved both in the crystal and in solution and has been shown to consist of a triple α-helical bundle (Johansson *et al.*, 2003; Gely *et al.*, 2010).

Sequence analyses predict a coiled-coil region within the *Paramyxovirinae* PMD (Karlin *et al.*, 2003; Habchi *et al.*, 2010). In agreement with this, the crystal structures of both *Sendai virus* (SeV) and MeV PMD consist of an elongated tetrameric coiled-coil structure (Tarbouriech, Curran, Ebel *et al.*, 2000; Tarbouriech, Curran, Ruigrok *et al.*, 2000; Communie *et al.*, 2013). Unexpectedly, while a combination of biochemical and biophysical studies showed that the *Nipah virus* (NiV) PMD adopts a trimeric coiled-coil conformation in solution (Blocquel *et al.*, 2013), recent X-ray crystallographic studies showed that it is tetrameric in the crystal (Bruhn *et al.*, 2014). The tetrameric coiled-coil organization of PMD has also been experimentally confirmed in the case of *Rinderpest virus* (RDV; Rahaman *et al.*, 2004), *human respiratory syncytial virus* (RSV; Llorente *et al.*, 2006, 2008) and *mumps virus* (MuV; Cox *et al.*, 2013). In the latter case, however, the tetramer was found to consist of two sets of parallel helices in opposite orientations, *i.e.* to be a dimer of two antiparallel coiled-coil dimers (Cox *et al.*, 2013).

Coiled coils are ubiquitous structures that most commonly consist of two, three or four α-helices wrapped around each other in a parallel or an antiparallel orientation to form 'supercoils' (Lupas & Gruber, 2005). Coiled coils are usually long, rigid oligomers with regular packing interactions and extended exposed surfaces. They are found in a diverse array of proteins from structural proteins such as keratin, myosin and collagen to transcription factors such as Fos and Jun (Burkhard *et al.*, 2001; Lupas, 1996). Interestingly, coiled coils may change their oligomeric state and conformation in response to environmental changes, an ability that is exploited most impressively in membrane fusion proteins, as illustrated by the structures of influenza haemagglutinin at neutral and acidic pH (PDB entries 2hmg and 1htm, respectively; Bullough *et al.*, 1994).

Here, we report a thorough structural characterization of MeV PMD both in solution and in the crystal. After having investigated the hydrodynamic properties and oligomeric state of an MeV PMD construct encompassing residues 304–375 using small-angle X-ray scattering (SAXS), size-exclusion chromatography (SEC) and cross-linking, we solved its crystal structure along with that of an additional shorter construct encompassing residues 304–360. Structural comparison between these two structures and a third one spanning residues 304–377, previously determined by Communie *et al.* (2013), showed that the structure of the protomers composing the coiled coils is fairly unchanged. However, significantly, differences were found in the quaternary coiled-coil structure, especially in its pitch, as well as in the 'knobs-into-holes' organization between the four protomers. Analysis of the crystal packing in terms of interaction energy between coiled coils showed that these structural differences essentially arise from different crystal arrangements, leading to significantly different interaction strengths.

2. Experimental procedures

2.1. Cloning of the PMD coding region

The PMD gene construct encoding residues 304–375 of the MeV P protein (strain Edmonston B) with an hexahistidine tag fused to its C-terminus was obtained by PCR using pET-21a/P_{H6} (Karlin, Longhi, Receveur *et al.*, 2002) as the template and *Pfu* polymerase (Promega). Primers (Operon) were designed to introduce *att*B1 and *att*B2 sites at the 5′ and 3′ ends, respectively, and to amplify the desired part of the P ORF with a fragment encoding a C-terminal hexahistidine tag. After digestion with *Dpn*I (New England Biolabs), the PCR product was purified (PCR Purification Kit, Qiagen) and cloned into the pDEST14 vector (Invitrogen) using the Gateway recombination system (Invitrogen).

The PMD gene construct encoding residues 304–360 of MeV P with a C-terminal hexahistidine tag (referred to as PMD-Ctrunc) was obtained by PCR using the plasmid pDEST14/PMD_{H6} as the template and a pair of mutagenic primers designed to introduce a hexahistidine tag-encoding fragment followed by a stop codon after position 360 of P. After digestion with *Dpn*I, the product was cloned into the pDEST14 vector.

Selection and amplification of the constructs was carried out using $CaCl_2$-competent *Escherichia coli* TAM1 cells (Active Motif). The sequence of the coding region of the constructs was checked by sequencing (GATC Biotech) and was found to conform to expectations.

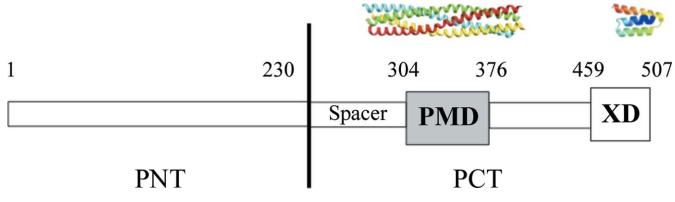

Figure 1
Domain organization of MeV P. Domain organization of P showing that it is composed of two moieties: PNT (amino acids 1–230) and PCT (amino acids 231–507). PCT consists of a disordered region (amino acids 231–303) referred to as the 'spacer', a structured region (amino acids 304–375) referred to as the PMD (P multimerization domain), a disordered linker (amino acids 376–458) and a globular region (amino acids 459–507) referred to as the X domain (XD). A ribbon representation of the crystal structures of MeV PMD (PDB entry 3zdo; Communie *et al.*, 2013) and XD (PDB entry 1oks; Johansson *et al.*, 2003) is shown.

2.2. Expression and purification of PMD constructs

The *E. coli* strain Rosetta (DE3) pLysS (Novagen) was used for expression. Cultures were grown overnight to saturation in LB medium containing 100 µg ml^{-1} ampicillin and 34 µg ml^{-1} chloramphenicol. An aliquot of the overnight culture was diluted 1/25 in SB medium and grown at 37°C. At an OD_{600} of 0.7, isopropyl β-D-1-thiogalactopyranoside (IPTG) was added to a final concentration of 0.2 m*M* and the cells were grown at 37°C for 3 h. The induced cells were harvested, washed and collected by centrifugation (5000*g*, 10 min). The resulting bacterial pellets were frozen at −20°C.

Expression of selenomethionine-substituted PMD was performed using the method of methionine-biosynthesis pathway inhibition (Doublié, 1997). Induction was carried out by adding 0.2 m*M* IPTG and incubating the cells overnight at 30°C.

The bacterial pellets containing either PMD or PMD-Ctrunc were resuspended in five volumes (*v*/*w*) buffer *A* (50 m*M* Tris–HCl pH 8, 300 m*M* NaCl, 20 m*M* imidazole, 1 m*M* phenylmethylsulfonyl fluoride) supplemented with 0.1 mg ml^{-1} lysozyme, 10 µg ml^{-1} DNAse I, 20 m*M* $MgSO_4$ and protease-inhibitor cocktail (Sigma; 50 µl per gram of cells). After a 20 min incubation with gentle agitation, the cells were disrupted by sonication (using a 750 W sonicator and five cycles of 30 s each at 60% power output). The lysate was clarified by centrifugation at 30 000*g* for 30 min and the clarified supernatant was injected onto a 5 ml HisTrap FF column (GE Healthcare) previously equilibrated in buffer *A* supplemented with 1 *M* NaCl. Elution was carried out using a gradient of imidazole in buffer *A* supplemented with 1 *M* NaCl. The fractions containing either PMD or PMD-Ctrunc were combined and loaded onto a Superdex 200 HR 16/60 column (GE Healthcare) and eluted in either 10 m*M* Tris–HCl pH 8, 5 m*M* EDTA or 10 m*M* bis-tris pH 6, 500 m*M* NaCl. The proteins were concentrated using a Centricon Plus-20 filter (molecular-weight cutoff of 3000 Da; Millipore) and stored at −20°C.

All purification steps, except for gel filtrations, were carried out at 4°C. The apparent molecular mass of the proteins eluted from the gel-filtration column was determined from a calibration carried out with LMW and HMW calibration kits (Amersham Pharmacia Biotech). Protein concentrations were calculated using the theoretical absorption coefficients ε (mg ml^{-1} cm^{-1}) at 280 nm obtained using the *ProtParam* program on the ExPASy server (http://www.expasy.org/tools).

2.3. Mass spectrometry (MALDI–TOF)

Mass analysis of the purified MeV PMD protein was performed using an AutoFlex II TOF/TOF. Spectra were acquired in the linear mode. Samples (0.7 µl containing 15 pmol) were mixed with an equal volume of sinapinic acid matrix solution, spotted onto the target and dried at room temperature for 10 min. The mass standard was myoglobin. Proteins were analyzed in the AutoFlex by matrix-assisted laser desorption ionization/time of flight (MALDI–TOF; Bruker Daltonics, Bremen, Germany).

2.4. Calculations of the hydrodynamic radius and the radius of gyration

The theoretical Stokes radius R_s (in Å) expected for a natively folded protein (R_s^{NF}) with an expected molecular mass MM_{theo} (in Da) was calculated according to (Uversky, 2002)

$$\log(R_s^{NF}) = 0.369\log(MM_{theo}) - 0.254. \quad (1)$$

The theoretical Stokes radius (R_s) of a natively folded tetramer ($R_s^{Tetram\ NF}$) was calculated as

$$\log(R_s^{Tetram\ NF}) = 0.369\log(MM_{theo} \times 4) - 0.254. \quad (2)$$

The theoretical Stokes radius (R_s) of a fully extended tetramer ($R_s^{Tetram\ FU}$) was calculated as

$$\log(R_s^{Tetram\ FU}) = 0.521\log(MM_{theo} \times 4) - 0.649. \quad (3)$$

The theoretical Stokes radius (R_s) of a tetramer adopting a premolten globule conformation ($R_s^{Tetram\ PMG}$) intermediate between that of a natively folded and that of a fully extended tetramer was calculated as

$$\log(R_s^{Tetram\ PMG}) = 0.403\log(MM_{theo} \times 4) - 0.239. \quad (4)$$

The theoretical radius of gyration (R_g; in Å) expected for a globular protein with a hydrodynamic radius R_s was calculated according to (Wilkins *et al.*, 1999)

$$R_g = (3/5)^{1/2}R_s. \quad (5)$$

The R_g of a thin rod with length L can be calculated as

$$R_g^2 = L_2/12. \quad (6)$$

MeV PMD consists of 78 residues, including the hexahistidine tag but excluding the initial methionine that is cleaved off. Using an average volume of 134 Å^3 per residue for proteins, the radius of a spherical tetramer with volume $V = (4/3)\pi R_s^3$ would be R_s = 21.5 Å. According to (5), the corresponding R_g is 16.65 Å.

2.5. Far-UV circular dichroism (CD)

CD spectra of MeV PMD were recorded on a Jasco 810 dichrograph using 1 mm thick quartz cells in 10 m*M* sodium phosphate pH 7 at 20°C either in the absence or the presence of 50% 2,2,2-trifluoroethanol (TFE). CD spectra were measured between 185 and 260 nm at 0.2 nm min^{-1} and were averaged from three independent acquisitions. Mean molar ellipticity values per residue (MRE) were calculated as MRE = $3300m\Delta A/(lcn)$, where l (the path length in cm) = 0.1, n (the number of residues) = 79, m (the molecular mass in Da) = 9040 and c (the protein concentration in mg ml^{-1}) = 0.1. Spectra were deconvoluted using the *DichroWeb* website (http://dichroweb.cryst.bbk.ac.uk; Whitmore & Wallace, 2004, 2008). The *CDSSTR* deconvolution method was used to estimate the α-helical content using reference protein set 7 (optimized for 190–260 nm).

In order to monitor protein unfolding, measurements at fixed wavelength (222 nm) were performed in the temperature range 20–100°C with a data pitch of 1°C and a temperature

slope of 1°C min^{-1}. The buffer solutions without the protein were used as blanks.

2.6. Cross-linking experiments

A fixed amount (5 µg) of MeV PMD in 30 µl of 50 m*M* HEPES pH 7.0, 150 m*M* NaCl buffer was incubated with suberic acid bis(*N*-hydroxysuccinimide ester) (SAB; Sigma) for 16 h at 20°C with different amounts of cross-linker (0–0.33 m*M*). The reactions were quenched by the addition of 100 m*M* glycine. The samples were analyzed by 15% SDS–PAGE followed by Coomassie Blue staining. SAB was first solubilized in DMSO at a concentration of 10 m*M* and then diluted in 50 m*M* HEPES pH 7.0, 150 m*M* NaCl to the desired concentration.

2.7. Crystallization and X-ray data collection of PMD and PMD-Ctrunc

Crystallization experiments were performed immediately after protein purification. Proteins were dissolved in 10 m*M* Tris–HCl, 5 m*M* EDTA. Screening experiments were carried out using the sitting-drop vapour-diffusion method at 20°C in 96-well Greiner crystallization plates using a nanodrop-dispensing robot (Mosquito Crystal; TTP Labtech) and various commercial crystallization kits (Molecular Dimensions, Emerald Bio and Jena Bioscience; Sulzenbacher *et al.*, 2002). Reservoir solutions were 150 µl in volume and crystallization drops were composed of 100, 200 or 300 nl protein solution at 10 mg ml^{-1} (PMD) or 5 mg ml^{-1} (PMD-Ctrunc) and 100 nl reservoir solution. Crystallization plates were sealed with transparent film after setup of the drops and were transferred to a storage cabinet at 20°C.

PMD crystals typically grew within 48 h to dimensions of 0.1 × 0.1 × 0.05 mm by mixing 300 nl protein solution at 10 mg ml^{-1} with 100 nl 10% PEG 8000, 0.1 *M* NaCl, 0.1 *M* 2-*N*-cyclohexylaminoethanesulfonic acid (CHES) pH 9.5. Single crystals were harvested from the drop and flash-cooled in liquid nitrogen at 100 K without any additional cryoprotectant. Several data sets were collected from PMD crystals on the PROXIMA1 beamline at SOLEIL, Gif-sur-Yvette, France using an ADSC Q315r detector at a wavelength of 0.97911 Å.

PMD-Ctrunc crystals grew within 5 days to dimensions of 0.2 × 0.1 × 0.05 mm by mixing 300 nl protein solution at 5 mg ml^{-1} with 100 nl 20% PEG 400, 0.2 *M* calcium acetate, 0.1 *M* 2-(*N*-morpholino)ethanesulfonic acid pH 5.5. Diffraction data were collected at a temperature of 100 K on beamline ID29 at ESRF, Grenoble, France to a resolution of 1.8 Å using a Pilatus 6M-F detector at a wavelength of 0.933 Å.

2.8. Structure determination, refinement and analysis

The data were integrated by *XDS* (Kabsch, 2010) and subsequently treated with *PHENIX* (Adams *et al.*, 2010) for scaling, molecular replacement and refinement. The *Coot* molecular-graphics software (Emsley & Cowtan, 2004) was used for model building. *PyMOL* (DeLano, 2002) and *UCSF Chimera* (Pettersen *et al.*, 2004) were used to visualize and draw the models.

The quality of the final MeV PMD and PMD-Ctrunc models was evaluated using *MolProbity* (Chen *et al.*, 2010; http://molprobity.biochem.duke.edu/). The *PDBeFold* server at EMBL–EBI (http://www.ebi.ac.uk/msd-srv/ssm/ssmstart.html) was used to compute root-mean-square deviations (r.m.s.d.s) between MeV PMD structures. Coiled-coil analysis was carried out using *TWISTER* (Strelkov & Burkhard, 2002), *SOCKET* (Walshaw & Woolfson, 2001) and *COILCHECK* (Alva *et al.*, 2008).

2.9. Small-angle X-ray scattering (SAXS) measurements and *ab initio* three-dimensional shape reconstructions

All SAXS measurements were carried out on beamline BM29 at the ESRF at a working energy of 12.5 keV, which corresponds to $\lambda = 0.992$ Å. The sample-to-detector distance of the X-rays was 2.847 m, leading to scattering vectors q ranging from 0.028 to 4.525 nm^{-1}. The scattering vector is defined as $q = 4\pi/\lambda\sin\theta$, where 2θ is the scattering angle. The exposure time was optimized to reduce radiation damage.

SAXS data were collected at 10°C using 30 µl protein solution at 1.11, 2.53, 3.28, 5.07 and 7.41 mg ml^{-1} in 10 m*M* Tris–HCl pH 8.5, 5 m*M* EDTA loaded in a fully automated sample charger. Ten exposures of 10 s each were performed for each protein concentration and were combined to give the average scattering curve for each measurement. Any data points affected by aggregation possibly induced by radiation damage were excluded. The profiles obtained at five different protein concentrations in the range 1.11–7.41 mg ml^{-1} had the same shape and were flat at low q values, indicating the absence of significant aggregation. We then used the highest concentration (7.41 mg ml^{-1}) to obtain the maximum information at high resolution.

Data reduction was performed using the established procedure available at BM29, and buffer background runs were subtracted from sample runs. The R_g and forward intensity at zero angle $I(0)$ were determined with the program *PRIMUS* (Konarev *et al.*, 2003) according to the Guinier approximation at low values, in a QR_g range up to 1.3,

$$\ln[I(Q)] = \ln(I_0) - (Q^2R_g^2)/3. \quad (7)$$

The forward scattering intensity was calibrated using BSA as a reference. The R_g and the pairwise distance distribution function, $P(r)$, were calculated with the program *GNOM*. The maximum dimension (D_{max}) value was adjusted such that the R_g value obtained from *GNOM* agreed with that obtained from the Guinier analysis.

Three-dimensional bead models were built by fitting the scattering data with the program *DAMMIF* (Franke & Svergun, 2009). 20 independent models were generated with *DAMMIF* assuming *P*4 symmetry. The models resulting from independent runs were superimposed using the *DAMAVER* suite (Volkov & Svergun, 2003). This yielded an initial alignment of structures based on their axes of inertia followed by minimization of the normalized spatial discrepancy (NSD),

which is zero for identical objects and greater than one for systematically different objects. The aligned structures were then averaged, giving an effective occupancy to each voxel in the model, and filtered at half-maximal occupancy to produce

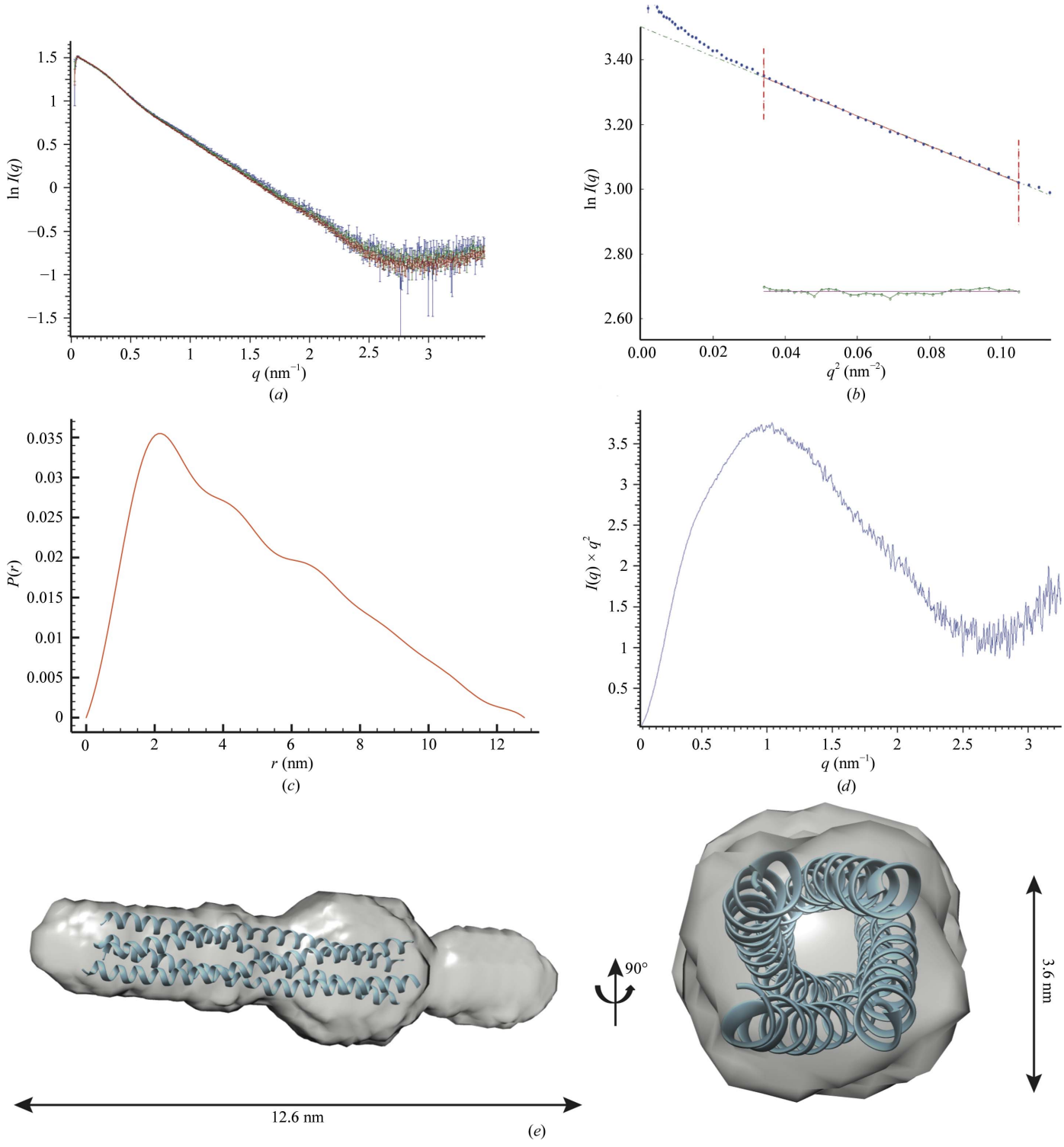

Figure 2
Small-angle scattering experiments on MeV PMD. (*a*) Experimental SAXS data recorded for q values up to 3.5 nm^{-1}. The curves obtained for three protein concentrations (1.11 g l^{-1}, blue; 3.28 g l^{-1}, green; 7.41 g l^{-1}, red) of peak 2 are represented after correction for concentration. (*b*) Representation of the Guinier plot for the protein at 7.41 g l^{-1}. (*c*) Pair distance distribution, $P(r)$, function of the data for the 7.41 g l^{-1}. (*d*) The Kratky plot corresponds to a protein with a folded and a disordered region. (*e*) Two orthogonal views of the *ab initio* envelope calculated with *DAMAVER*. 20 *DAMMIF* calculations were performed and averaged with *DAMAVER* to produce the averaged and filtered shape shown in grey. The crystal structure of MeV PMD-Ctrunc (blue) is shown within the SAXS-derived model. Docking of the model in the envelope was performed manually using *PyMOL*.

models of the appropriate volume that were used for all subsequent analyses.

3. Results

3.1. Hydrodynamic properties and oligomeric state of MeV PMD as inferred from size-exclusion chromatography and cross-linking studies

The recombinant PMD protein was purified to homogeneity (>95%) in two steps: immobilized metal-affinity chromatography (IMAC) and size-exclusion chromatography (SEC) (Supplementary Figure S1[1]). PMD consistently eluted from the SEC column as two peaks: a major peak with an apparent molecular mass of 236 kDa and a second peak with an apparent molecular mass of 63.5 kDa (Supplementary Fig. S1). These apparent molecular-mass values are both well above the expected value for a tetramer (≃36 kDa). The R_s values of peaks 1 and 2, as inferred from their apparent molecular masses, are 53.5 and 33 Å, respectively (Uversky, 2002). These values are much and slightly larger, respectively, than the value expected for a globular and compact tetramer (26.8 Å; Uversky, 2002), and can in principle be attributed to the elongated shape of the MeV PMD structure (Communie *et al.*, 2013). Note that the elution profile was found to be independent of the protein concentration, the pH and the NaCl concentration. Notably, when peak 2 was re-injected onto the SEC column it again gave rise to two peaks, likely reflecting either the fact that the two peaks are not well resolved or the existence of an equilibrium between the two forms (data not shown). The homogeneity of both PMD peaks was checked by mass spectrometry (MALDI–TOF) experiments, which showed the presence of a major species at 8914 ± 5 Da in both cases, a value that fits perfectly with the expected molecular mass (8909 Da) for a protein in which the initial methionine has been cleaved off.

In agreement with the tetrameric organization of MeV PMD (Communie *et al.*, 2013), cross-linking experiments carried out on both PMD peaks using SAB, a bifunctional reagent of fixed size (13.1 Å) that reacts with lysine, resulted in the formation of dimers, trimers and tetramers (Supplementary Fig. S2). Increasing cross-linker concentrations resulted in the accumulation of tetramers, with no concomitant appearance of higher-order oligomers (Supplementary Fig. S2).

3.2. Far-UV CD studies

The far-UV CD spectra of peaks 1 and 2 are quite similar to each other, supporting an overall similar secondary-structure content (Supplementary Fig. S3*a*). The spectra are typical of folded proteins with a high (*i.e.* >55%) helical content and display an ellipticity ratio at 222 and 208 nm ($\Theta_{222/208}$) of greater than 1.0 (Supplementary Fig. S3*a*), a value indicative of the presence of interacting helices, as previously observed in the case of SeV, RDV and NiV PMDs (Tarbouriech, Curran, Ebel *et al.*, 2000; Rahaman *et al.*, 2004; Blocquel *et al.*, 2013). Notably, although no significant variation in the secondary-structure content was observed upon the addition of 50% TFE, the $\Theta_{222/208}$ ratio falls below 1 (Supplementary Fig. S3*a*). Because high TFE concentrations are known to disrupt tertiary and quaternary structure and to stabilize secondary structure (Lau *et al.*, 1984), these results confirm that MeV PMD forms tetramers through coiled-coil interactions.

To assess the thermal stability of MeV PMD tetramers, for both peaks we plotted the MRE at 222 nm (MRE_{222}) as a function of temperature (Supplementary Fig. S3*b* and data not shown). MeV PMD displays an unfolding profile typical of a two-state cooperative transition, with an apparent melting temperature (T_m) of approximately 75°C. Note that at 100°C the MRE_{222} value is still negative (−5000), in agreement with the presence of residual α-helices (Supplementary Fig. S3*b* and data not shown). Following stepwise cooling from 100°C to 20°C, the final MRE_{222} at 20°C is very similar to that of the initial spectrum before heating, which indicates the reversibility of thermal unfolding and argues for refolding of the main structural motif (*i.e.* the coiled coil). In addition, the renaturation curve is close to the denaturation curve, indicating reciprocal temperature-induced denaturation–renaturation (Supplementary Fig. S3*b* and data not shown).

Based on these results, we propose that the two peaks observed in SEC analyses both correspond to folded conformations adopting a very elongated coiled-coil structure and displaying a high thermal stability.

Table 1
Molecular dimensions of PMD calculated from SAXS experiments.

Protein concentration (g l^{-1})	R_g (Guinier) (Å)	$I(0)$ (Guinier) (cm^{-1})	D_{max} (Å)
1.11	38.1 ± 0.4	29.5 ± 0.2	132
2.53	37.9 ± 0.2	29.8 ± 0.9	126
3.28	37.8 ± 0.2	32.3 ± 0.7	128
5.07	39.1 ± 0.7	33.7 ± 0.5	126
7.41	37.9 ± 0.8	34.3 ± 0.4	126

3.3. Small-angle X-ray scattering (SAXS) studies

We carried out SAXS measurements on both MeV PMD peaks. The shapes of the SAXS profiles (Fig. 2*a*) and the corresponding Guinier plots (Fig. 2*b*) obtained with peak 2 are independent of protein concentration, indicating the absence of significant aggregation. Notably, the curves and Guinier profiles obtained with peak 1 (data not shown) were very similar, confirming that peak 2 is in equilibrium with peak 1. Guinier analysis in the low-q region gives an R_g of 38.2 ± 0.11 Å (see Table 1), which is in agreement with the value of 39.1 ± 0.07 Å determined from the pair distribution function $P(r)$ (see Table 1). This R_g value is significantly larger than that expected for a globular tetramer of the same molecular mass (16.65 Å; see §2), which is in agreement with the overall elongated structure of MeV PMD (Communie *et al.*, 2013).

The molecular mass calculated from the forward scattering intensity $I(0)$ is 37.34 kDa (see Table 1), a value similar to that

[1] Supporting information has been deposited in the IUCr electronic archive (Reference: DZ5322).

expected for a tetrameric form (36.16 kDa). The distance distribution function inferred from the scattering curve of MeV PMD exhibits a maximum at 20 Å, two shoulders at 42 and 63 Å, respectively, and a long tail to 126 Å (D_{max}) typical of an elongated object with multiple domains (Fig. 2*c*). The R_g of a thin rod of length $L = 126$ Å is 36.4 Å (see §2), a value that is in very good agreement with the values estimated from both the Guinier plot and the pair distribution function.

The Kratky plot presents a maximum at 10 Å and a flat region above 25 Å (Fig. 2*d*). The shape of the plot is indicative of a structured protein with a disordered appendage, as judged from the bell-shaped nature of the curve, which displays a clear maximum, and from the presence of the flat region.

Taking into consideration the fact that SAXS studies unveiled that MeV PMD is a tetramer possessing a disordered moiety, we propose that the two peaks observed in SEC could reflect different degrees of compaction of the tetramer, with peaks 1 and 2 possibly corresponding to a very extended and a more compact form, respectively. In support of this hypothesis, the experimentally observed R_s for peak 1 (53.5 Å) is very similar to the value (53.2 Å) expected for a tetramer of the same mass as MeV PMD adopting a fully extended conformation (see §2), while the R_s of peak 2 (33 Å) is similar to the value expected (39.6 Å) for a tetramer with an intermediate conformation whose compaction is greater than that of a fully extended form but lower than that of a globular compact tetramer (see §2).

3.4. X-ray diffraction studies and structural models of MeV PMD

Although both peaks 1 and 2 yielded crystals, better quality crystals were invariably obtained with peak 2. Initially, we crystallized the MeV PMD protein and measured many X-ray diffraction data sets from several crystals. Our attempts at obtaining a high-quality structure using either molecular replacement with the SeV PMD tetramer as a template (PDB entry 1ezj; Tarbouriech, Curran, Ruigrok *et al.*, 2000) or SAD using synchrotron data collected from crystals of selenomethionine-substituted protein failed. This was owing to significant translational pseudosymmetry problems induced by the presence of a disordered C-terminal region encompassing residues 360–375. In order to overcome this problem, we designed a slightly shortened form of MeV PMD, referred to as PMD-Ctrunc, encompassing residues 304–360 of P. PMD-Ctrunc was purified to homogeneity by IMAC and SEC (Supplementary Fig. S1). Unexpectedly, the protein was found to elute from the SEC column in the excluded volume (Supplementary Fig. S1), which suggests either a higher-order oligomerization combined with an elongated shape or protein aggregation. In spite of this, and to our great surprise, MeV PMD-Ctrunc was able to readily crystallize. This truncated form allowed us to obtain an initial structure, which was subsequently used as a model to obtain the structure of the entire MeV PMD.

3.4.1. PMD-Ctrunc X-ray crystal structure. The data were initially indexed by *XDS* with very good statistics in space group *I*422, but suffered from poor intensity statistics (*L*-test) as shown by *phenix.xtriage*. In addition, a large off-origin Patterson peak with an amplitude of 40% of the origin peak was present. Despite these problems, the data were phased in space group *I*422 by molecular replacement (*Phaser-MR* in *PHENIX*) using a fragment of the SeV phosphoprotein tetramer (PDB entry 3zdo; Communie *et al.*, 2013) as the search model. An initial model structure of the MeV PMD-Ctrunc protein was then constructed manually using *Coot* during iterative runs of *phenix.refine* and *phenix.autobuild*. However, the R_{free} factor remained high at around 40%. This led us to consider the possibility that the *I*422 symmetry was an artefact induced by the presence of twinning as well as pseudo-translational symmetry problems. Nevertheless, this procedure enabled us to construct a better molecular model for further molecular-replacement trials in lower symmetry groups. The best molecular-replacement and refinement statistics were obtained in space group $P12_11$, with one tetramer in the asymmetric unit (two tetramers in the entire unit cell) and with fairly good R_{free}-factor (24%), molecular-geometry, Ramachandran-plot and rotamer-analysis statistics (see Table 2). The structure was resolved for amino acids 307–360 and was deposited in the PDB as entry 4bhv.

Table 2
Crystallographic data-collection and refinement statistics.

Values in parentheses are for the outer resolution bin.

	PMD (amino acids 304–375)	PMD-Ctrunc (amino acids 304–360)
Data collection		
X-ray source	PROXIMA1, SOLEIL	ID29, ESRF
Wavelength (Å)	0.979110	0.976254
Space group	*P*1 [No. 1]	$P12_11$ [No. 4]
Unit-cell parameters		
a (Å)	34.34	33.08
b (Å)	34.39	33.62
c (Å)	139.69	99.14
α (°)	97.04	90.00
β (°)	96.90	96.75
γ (°)	90.12	90.00
Resolution range (Å)	45.87–2.15 (2.27–2.15)	32.84–2.10 (2.21–2.10)
Completeness (%)	96.3 (88.7)	98.5 (98.5)
R_{merge} (%)	0.097 (0.576)	0.092 (0.152)
R_{meas} (%)	0.116 (0.695)	0.109 (0.181)
$R_{p.i.m.}$ (%)	0.063 (0.385)	0.057 (0.096)
Mean $I/\sigma(I)$	8.3 (2.3)	9.8 (6.2)
Total reflections	109139 (13856)	43085 (6085)
Unique reflections	32947 (4408)	12725 (1838)
Multiplicity	3.3 (3.1)	3.4 (3.3)
Average mosaicity	0.35	0.41
Refinement		
R_{work} (%)	0.25 (0.33)	0.23 (0.36)
R_{free} (%)	0.30 (0.35)	0.24 (0.34)
No. of atoms	3730	2067
No. of residues	420	228
Ramachandran favoured (%)	99	98
Ramachandran outliers (%)	0	0.45
R.m.s.d., bonds (Å)	0.007	0.013
R.m.s.d., angles (°)	1.02	1.19
Clashscore	9.50	11.61
Mean *B* factor, protein (Å^2)	20.60	16.20
Mean *B* factor, ligands (Å^2)	—	26.00
Mean *B* factor, solvent (Å^2)	22.70	19.60

It is worth noting the following. (i) In space group $P12_11$ the data showed twinning problems, with one twofold pseudo-merohedral operator (h, $-k$, $-h-l$) with an estimated twin fraction of 20%, and a significant off-origin Patterson peak of 35% ($p = 5.6249 \times 10^{-4}$) of the origin peak, indicating pseudo-translational symmetry. (ii) Many cycles of refinement were necessary using the twin target function (h, $-k$, $-h-l$) before an acceptable $R_{\rm free}$ factor of 28% was reached. Successive geometry corrections and refinement cycles without the twin target function then gave the final $R_{\rm free}$ factor of 24%. (iii) A solution with a higher $R_{\rm free}$ factor (29%) was also obtained by the same procedure in space group $P1$ with two tetramers in the unit cell.

The PMD-Ctrunc structure contains a Ca^{2+} ion located in the inner channel of the coiled coil coordinated by four Asn residues (Fig. 3*a*). In the final model, each protomer consists of an α-helix of 86–89 Å in length encompassing 54 residues and extending over 15 turns (Figs. 3*a* and 3*b*). In all protomers, the α-helix is kinked at Leu342 at the end of a four-leucine motif. Part of the experimental electron-density map is shown in Fig. 3(*c*). The tetramer is formed through a coiled coil involving the long helix of each protomer. The electrostatic surface of the tetramer calculated by *APBS* (Baker *et al.*, 2001) is mainly polar, with a basic patch consisting of Lys350, Lys351 and Asn354 being observable towards the C-terminal end of the tetramer (Fig. 3*d*).

3.4.2. PMD X-ray crystal structure. The PMD crystals presented the same problems as discussed above for the PMD-Ctrunc crystals. In particular, the data showed twinning problems with several pseudo-merohedral twin operators (two fourfold and five twofold) with twin fractions of 40% as well as an important off-origin Patterson peak of 20% ($p = 8 \times 10^{-3}$) of the origin peak, indicating pseudo-translational symmetry. Note that the data were initially indexed by *XDS* with very good statistics in space group $I422$, but suffered from poor intensity statistics (L-test). Further molecular replacement and refinement of solutions in this space group failed. We therefore phased the data in space group $P1$ by molecular replacement (using *Phaser-MR* in *PHENIX*) with two tetramers in the unit cell using the PMD-Ctrunc tetramer (PDB entry 4bhv) as the model. Statistics for the data collection and refinement of the structure are given in Table 2. Refinement was performed by taking into account a twin target function (h, $-k$, $-h-l$) until an $R_{\rm free}$ of 30% was reached. Successive geometry corrections and refinement cycles without the twin target function gave a final $R_{\rm free}$ of 29%. Only amino acids 308–357 were resolved in this structure, while the rest of the polypeptide chain, *i.e.* amino acids 358–375, was disordered. Atomic coordinates and structure-factor amplitudes have been deposited in the PDB as entry 4c5q. SAXS measurements, and in particular the Kratky plot (see Fig. 2*d*), confirmed the presence of a disordered region in the protein before crystallization.

As in the case of PMD-Ctrunc, a kink at Leu342 occurs in all chains of both tetramers, and a patch of three exposed basic residues (Lys350, Lys351 and Asn354) is present in both tetramers. Interestingly, a similar kink is also observed in the NiV and

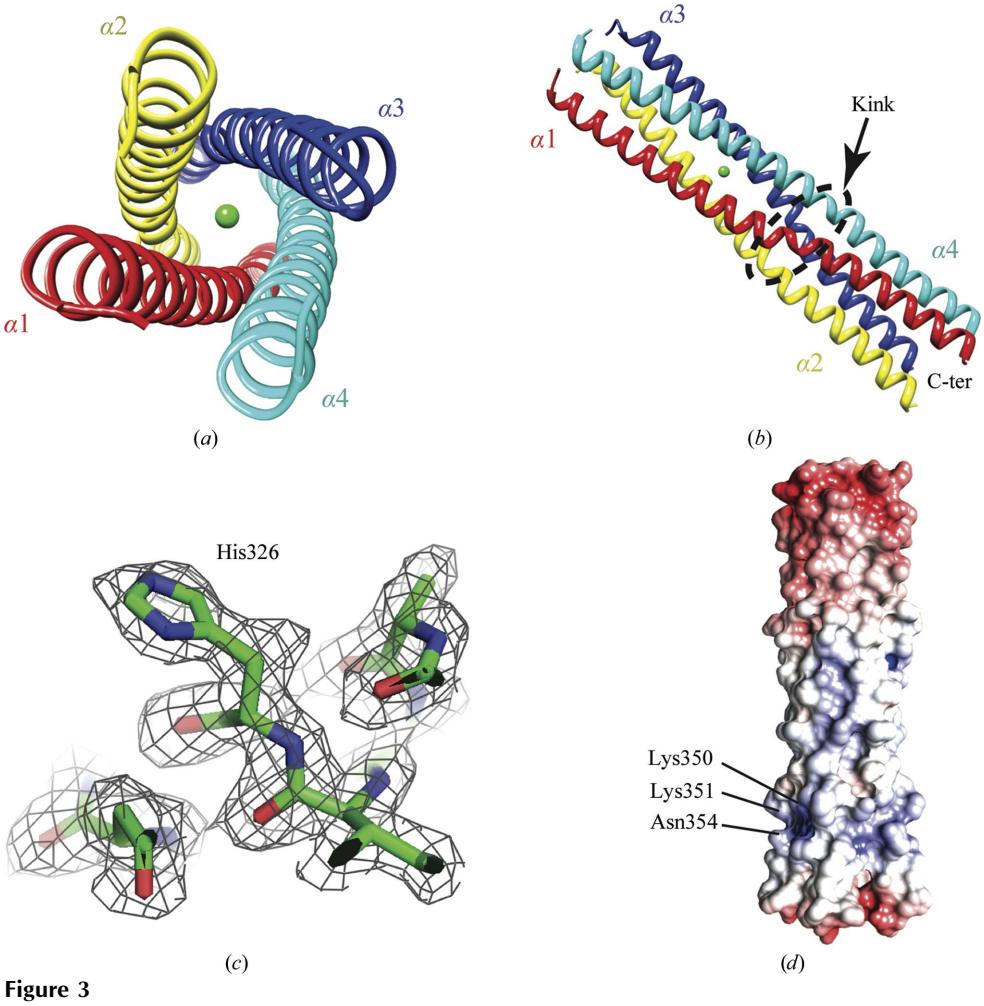

Figure 3
Structure of MeV PMD-Ctrunc. (*a*, *b*) Two views of the MeV PMD-Ctrunc model (ribbon representation), in which each monomer is shown in a different colour. A calcium ion located in the channel of the coiled coil and coordinated by four Asn residues is shown in green. The arrow indicates the kink occurring at Leu342. (*c*) A representative part of the $2F_o - F_c$ electron-density map contoured at 1σ. (*d*) An electrostatic surface potential representation of the MeV PMD-Ctrunc tetramer. The patch of basic residues functionally corresponding to those observed in the SeV (Tarbouriech, Curran, Ruigrok *et al.*, 2000) and NiV (Bruhn *et al.*, 2014) PMD structures is highlighted.

Table 3
R.m.s.d.s. among the MeV and SeV PMD structures.

The numbers in parentheses indicate the number of C^{α} atoms included in the structural alignment.

	4bhv (MeV)	4c5q (MeV)	3zdo (MeV)	1ezj (SeV)
4bhv		1.315 (54)	1.374 (57)	1.811 (56)
4c5q	1.319 (54)		1.188 (54)	1.833 (50)
3zdo	1.353 (57)	1.177 (54)		1.862 (54)
1ezj	1.811 (56)	1.828 (50)	1.865 (54)	

MuV tetramers (Cox *et al.*, 2013; Bruhn *et al.*, 2014) but not in the SeV structure (Tarbouriech, Curran, Ruigrok *et al.*, 2000).

3.4.3. SAXS model of MeV PMD. We also generated a SAXS-derived low-resolution model of MeV PMD, to which we fitted the structure of MeV PMD-Ctrunc. To this end, we employed the program *DAMMIF* to carry out *ab initio* shape reconstruction from the SAXS data. The bead models generated appear as elongated cylinders, in agreement with the coiled-coil organization of MeV PMD. The models resulting from 20 independent runs imposing *P*4 symmetry were superimposed using the *DAMAVER* suite. The models were highly reproducible, with an average normalized spatial discrepancy (NSD) of 0.570 ± 0.029, indicating structurally similar solutions. Furthermore, all of the models were similar in terms of agreement with the experimental data, as judged from the *DAMMIF* χ parameter and the quality of the fit to the experimental curve. The high-resolution structure of the MeV PMD-Ctrunc tetramer could easily be accommodated in the average model generated by *DAMAVER*, with the additional density potentially being able to accommodate the missing residues, *i.e.* residues 361–375, that could not be modelled in the crystal structure (Fig. 2*e*).

3.5. Structural comparison among MeV PMD structures

The most striking result provided by the X-ray diffraction data is a significant difference in the tetrameric coiled-coil geometry between the PMD and PMD-Ctrunc structures. In the following, we quantify this difference and also compare our MeV PMD structures with that reported by Communie *et al.* (2013).

Fig. 4(*a*) depicts the three PMD structures, and Fig. 4(*b*) displays their superimposition, as obtained using *CHIMERA* with the *MatchMaker* function (Meng *et al.*, 2006), resulting in r.m.s.d. values of between 1.2 and 1.4 Å over 50 aligned residues (Table 3). Noteworthy, these rather high r.m.s.d. values

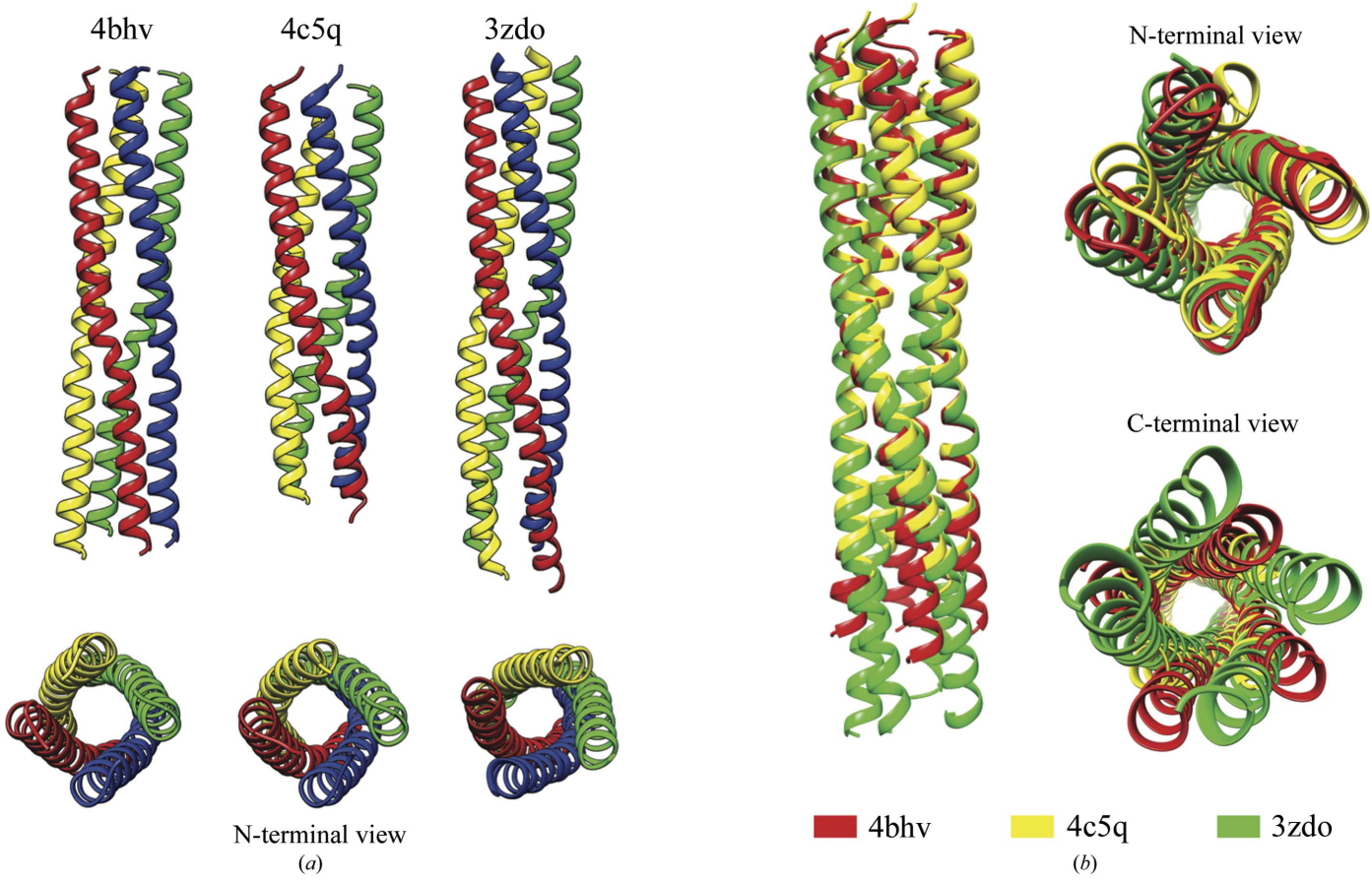

Figure 4
Structural comparison among MeV PMD structures. (*a*) Ribbon representations of the crystal structures of the MeV PMD tetramers as observed in the three different MeV PMD forms solved to date. (*b*) Superimposition of the three MeV PMD tetramers, with PDB entries 4bhv, 4c5q and 3zdo shown in red, yellow and green, respectively.

Table 4
Values for the main structural coiled-coil parameters determined by *TWISTER*.

Protein	Coiled-coil radius r_0 (Å)	Coiled-coil pitch (Å)	Residues per turn (Å)	Rise per residue (Å)
PMD-Ctrunc, 4bhv	7.57	231.9	3.56	1.52
PMD, 4c5q	7.44	158.7	3.58	1.54
PMD, 3zdo	7.49	179.2	3.57	1.54

arise from differences in the quaternary structure and do not reflect differences between the α-helical protomers, with typical r.m.s.d. values ranging in this case between 0.6 and 0.8 Å over 50 aligned residues (data not shown). The finding that the three PMD structures differ in the relative arrangement of their protomers underscores the ability of closely related forms of the same protein, differing only in their C-terminal boundaries and in the crystallization conditions, to assemble into slightly different coiled-coil structures. The variations in the quaternary structure are better displayed in Supplementary Movies S1, S2 and S3, corresponding to three different views of a morphing made with the three structures. The tetramers in the three MeV PMD structures are similarly hydrophobic, with only a few charged/polar residues and water molecules in their channels.

The most important discrepancies between these coiled coils are observed in the C-terminal region. In particular, in the case of the PMD-Ctrunc structure the four protomers appear to be more distant from each other compared with the other two PMD structures, leading to a larger inner diameter. Furthermore, while in the two MeV PMD structures described here (*i.e.* PDB entries 4bhv and 4c5q) the kink occurring at Leu342 is conserved in all chains, in the structure reported by Communie and coworkers the kink does not occur in all chains, being absent in chains *C* and *F* of tetramers 1 and 2, respectively.

In order to understand the physical origin of these discrepancies, we have undertaken a detailed analysis of (i) the local structural parameters of the coiled-coil structure measured by X-ray diffraction, (ii) the tetramer organization in terms of 'knobs-into-holes packing' and (iii) the mechanical constraints imposed by the crystal packing of each tetramer within the crystal by calculating the interaction energy between protomers within the coiled-coil structure as well as the interaction energy between close neighbouring tetramers in the crystal.

3.5.1. Local coiled-coil parameters. For each MeV PMD structure, Table 4 shows the radius, the pitch, the number of residues per turn and the rise of the coiled coil per residue as obtained using the *TWISTER* program (Strelkov & Burkhard, 2002). The radius is the mean distance between the centre of the quaternary helix and the C^{α} atoms. The most striking difference concerns the pitch, with the PMD-Ctrunc structure exhibiting a pitch that is 30% higher than that of PMD with PDB entry 3zdo and 45% higher than that of PMD with PDB entry 4c5q (see Table 4). In practice, this means that the PMD-Ctrunc tetramer is significantly less twisted, reflecting a less tight association of the four protomers within the coiled coil.

3.5.2. 'Knobs-into-holes' packing. The hallmark of most coiled coils is a regular sequence pattern known as the 'heptad repeat', in which the first and fourth positions (positions *a* and *d* in the *abcdefg* heptad repeat) correspond to hydrophobic residues. The stability of the quaternary coiled-coil organization is obtained by a 'knob-into-hole' geometry in which a residue from one helix (the knob) packs into a space surrounded by four side chains of the facing helix (the hole). Despite this apparent simplicity at the sequence level, coiled coils display a considerable degree of structural diversity.

The significant deformation of the PMD-Ctrunc coiled coil prompted us to address the question as to whether this deformation could also give rise to differences in the 'knobs-into-holes' arrangement. To this end, we used the *SOCKET* program (Walshaw & Woolfson, 2001).

For each structure, we first identified the positions of all knobs present in each protomer (see Supplementary Table S1). We then identified the knobs conserved in all four protomers of a tetramer (Fig. 5). These analyses revealed a difference in the organization of knobs, with the structure determined by Communie and coworkers (PDB entry 3zdo) exhibiting unique properties. Indeed, in this latter case, comparatively few knobs are conserved from one protomer to another within the same tetramer. Detailed analysis of knobs in chains *A*, *B*, *C* and *D* within the three structures led to the identification

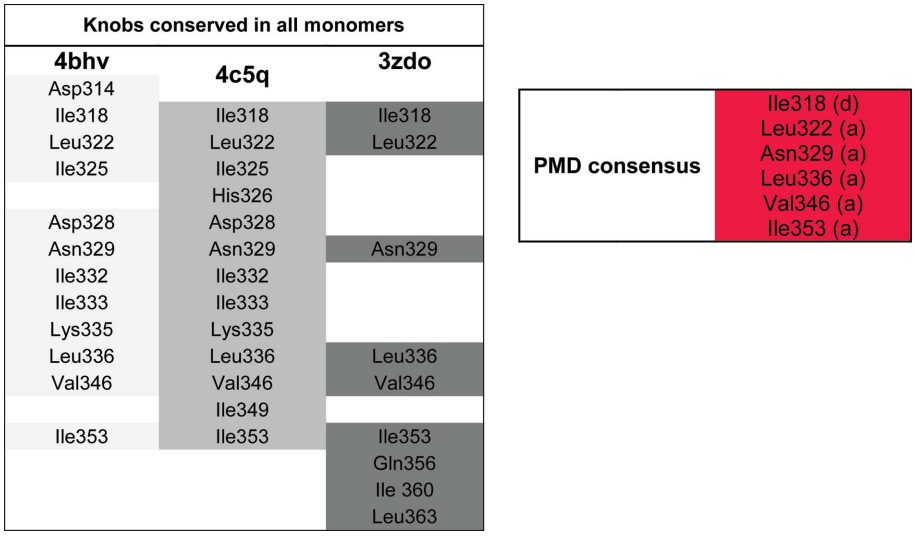

Figure 5
Knobs-into-holes analysis with the *SOCKET* program. The residues serving as knobs in the four different chains of a tetramer and in the various MeV PMD structures are listed. The 'consensus' panel shows the six residues that are strictly conserved in all structures.

of six conserved knobs (Fig. 5). Five out of these six knobs correspond to residues in the *a* position of heptad repeats, while residue Ile318 falls at position *d*. The conservation of the *a* and *d* residues confirms their role in building up the backbone of coiled coils and in ensuring their cohesion.

3.5.3. Crystal packing. Fig. 6 shows the crystal-packing arrangement of the three structures. Tetramers are packed in a parallel manner along their length, forming stacks along the *a* and *b* directions. These stacks are repeated along the *c* direction. The distance between these stacks in the *c* direction in the case of the PMD with PDB entry 4c5q is remarkably large, 56 Å, compared with the tetramer length, which is 73 Å. Note that the inter-stack distance in the *c* direction in the case of the other two PMDs is 13 Å (PMD-Ctrunc; length 84 Å) and 26 Å (PDB entry 3zdo; length 95 Å). The large empty space of PMD with PDB entry 4c5q is occupied by the disordered C-terminal region of the protein (amino acids 358–375).

From this picture, it is clear that the PMD-Ctrunc structure is the most tightly packed in all directions. The mean distance between adjacent tetramers within the crystal is given in Table 5 together with their lengths and diameters. Lengths and distances between close neigbouring tetramers were measured using *UCSF Chimera*. More precisely, these distances were calculated by taking into account the volume enclosed by the 'interface surface' between adjacent tetramers. The 'interface surface' is defined here as the surface that divides the space between atoms belonging to the closest neighbouring

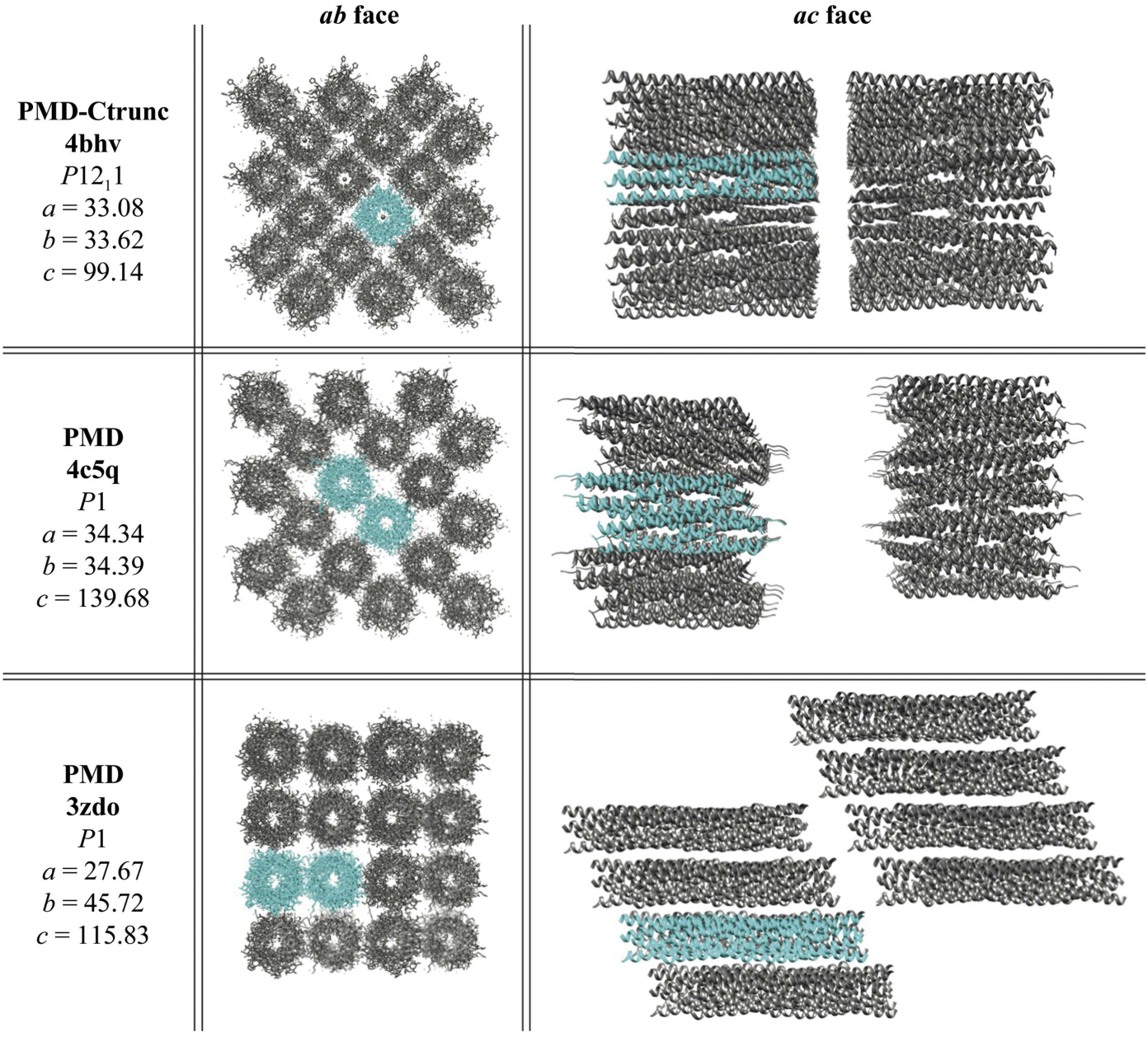

Figure 6
Crystal packing of the three MeV PMD structures (PDB codes 4bhv, 4c5q and 3zdo). The molecule(s) of the asymmetric unit is (are) shown in cyan.

Table 5
Physical properties of each tetramer calculated with *CHIMERA*.

	Tetramer length (Å)	Tetramer diameter (Å)	Distance between tetramers (Å)
PMD, 4c5q	72.6 ± 2.5	20.1 ± 2.5	56.3 ± 2.5
PMD-Ctrunc, 4bhv	84.2 ± 2.5	21.0 ± 2.5	13.1 ± 2.5
PMD, 3zdo	95.47 ± 2.5	20.6 ± 2.5	25.9 ± 2.5

Table 6
Stabilization energy calculated with *COILCHECK*.

Stabilization energy per residue in kJ mol^{-1}.

	E_{self} within a single tetramer	E_{inter} between two tetramers in the unit cell	E_{total} in the unit cell (E_{self} + E_{inter})
PMD, 4c5q	−13.46	+2.43	−22.06
PMD-Ctrunc, 4bhv	−6.20	−13.68	−39.76
PMD, 3zdo	−12.05	−2.31	−28.72

tetramers. The division of space is based on the Delaunay tetrahedralization (Delaunay, 1934), as used by the 'intersurf' routine in *UCSF Chimera*. Calculation of the 'interface surface' in our case was performed by considering a tetramer surrounded by eight neighbours. The mean distance between tetramers is calculated by considering the volume V enclosed by the 'interface surface' and by considering the corresponding mean diameter D by the simple relation $V = \pi D^2 L/4$ (the volume of a cylinder with diameter D and length L). From the resolution of the structures, we estimated the mean error in length and distance measurements to equal 2.5 Å.

In order to obtain a more precise idea about the interactions and the resulting mechanical stresses and strains within the crystal, we used the *COILCHECK* program (Alva *et al.*, 2008). This latter calculates the strength of interactions between two helices involved in coiled coils on the basis of noncovalent interactions. The energy that stabilizes coiled coils arises from (i) intra-chain and inter-chain hydrogen-bonding energy, (ii) inter-chain van der Waals interactions (hydrophobic interactions and short contacts) and (iii) inter-chain electrostatic interactions. For any given coiled coil, *COILCHECK* calculates the energy values for the interactions listed above and sums them to obtain the total inter-protomer stabilizing energy (E_{total}), which is divided by the total number of residues to obtain the energy per residue. Table 6 gives the stabilization energies (in kJ mol^{-1}) within each tetramer (E_{self}) and between two adjacent tetramers (E_{inter}), as well as the total stabilization energy inside the unit cell. This analysis unveiled that all of the MeV PMD tetramers are energetically stable, which is in agreement with the high melting temperature determined in the CD studies. The most stable tetramer is PMD with PDB code 4c5q, with a stabilization energy of −13.56 kJ mol^{-1} (see Table 6). This finding is in agreement with the pitch of this tetramer, which was found to be the smallest (see Table 4) and hence corresponds to a tightly packed tetramer. However, in the case of this PMD structure the stabilization energy between tetramers in the unit cell is found to be positive (E_{inter} = 2.43 kJ mol^{-1}), which is rather surprising. The discrepancy may arise from the fact that *COILCHECK* only takes into account amino acids 304–357, *i.e.* those residues that are effectively present in the resolved PMD structure. The remaining residues are disordered but do account for the stability of the crystal. Finally, the total stabilization energy in the unit cell shows that the most stable crystal is PMD-Ctrunc, which is in agreement with the previously discussed observations concerning the crystal packing.

4. Discussion and conclusions

4.1. MeV PMD exists in a dynamic equilibrium between two forms differing in compaction

MeV PMD consistently eluted from the SEC column as two peaks, the apparent molecular masses, and corresponding R_s values, of which are above the values expected for a tetramer. Since SAXS measurements provided a molecular mass that was in close agreement with that expected for a tetramer, and at the same time revealed that the protein consists of a structured moiety and of an at least partly disordered appendage, we reasoned that the two peaks could reflect different degrees of compaction of an elongated tetramer. This hypothesis is corroborated by structural data that indicated the presence in the MeV PMD structure of a disordered C-terminal region encompassing 18 residues. It is tempting to speculate that peak 1 could represent a more disordered conformation, in which the flexibility of the C-termini would lead to a broadening of the molecule at its C-terminal extremity, while peak 2 could correspond to a more folded and hence compact form. The fact that the CD studies did not point out any significant differences in the secondary-structure content and thermostability between the two peaks is likely to reflect the existence of a dynamic equilibrium between the two peaks.

Strikingly, such very large values of the apparent molecular mass and R_s were not reported for the cognate PMDs from SeV, RDV and NiV, as these were found to have molecular masses that were either consistent with or only moderately higher than the values expected for tetrameric (SeV and RDV) or trimeric (NiV) forms (Tarbouriech, Curran, Ebel *et al.*, 2000; Rahaman *et al.*, 2004; Blocquel *et al.*, 2013). However, previous sedimentation-velocity studies which were carried out on a trypsin-resistant fragment of the RSV P protein (referred to as fragment X and encompassing residues 104–163) showed the presence of a major peak corresponding to a tetramer (30 kDa) and of an additional peak at 56 kDa (Llorente *et al.*, 2008). Furthermore, a smaller (4.5 kDa) trypsin-resistant fragment of the RSV P protein (referred to as fragment Y* and being the functional counterpart of residues 332–375 of MeV P) was found to elute from a SEC column as a peak with an apparent molecular mass of 120 kDa (Llorente *et al.*, 2008). This behaviour was ascribed to the very elongated shape of the RSV P tetramer, a conclusion also supported by the high frictional ratio of the X fragment (Llorente *et al.*, 2008).

4.2. Residual disorder in MeV PMD structures

In the final MeV PMD model (PDB entry 4c5q), only amino acids 308–357 could be resolved in the structure, with downstream residues being disordered. Although this finding is in agreement with SAXS measurements indicating the occurrence within MeV PMD of a disordered region in solution, it is in striking contrast to the observations of Communie and coworkers, who could model a region extending up to residue 372 in the electron density (Communie *et al.*, 2013). The more ordered nature of the C-terminal region of this latter structure is likely to explain the higher apparent T_m (85°C) compared with that reported here.

The disordered nature of residues 358–375 explains our failure to solve the structure of MeV PMD by SAD using selenomethionine-substituted crystals, as the only methionine residue (*i.e.* Met371) remaining in the protein after cleavage of the initial methionine falls in this disordered region. Notably, while residues 358–360 could be modelled in the electron density in the MeV PMD-Ctrunc structure, they are disordered in the structure of MeV PMD, suggesting that the presence of the downstream long flexible appendage (residues 361–375) imparts flexibility to the neighbouring upstream residues, which are otherwise less mobile in the shorter form.

4.3. Structure determination of coiled coils is challenging

Determination of the crystal structure of MeV PMD was found to be rather challenging, as illustrated well here and also in previous studies by Communie and coworkers. Indeed, in both cases the structure could not be solved using the entire SeV or MeV tetramer as the search model, and rather needed either an *ab initio* molecular-replacement procedure using a large pool of different helices generated with *Flexible-Meccano* (Communie *et al.*, 2013) or the use of a fragment of the SeV tetramer as the search model (this study). Strikingly, and likewise, attempts at solving the crystal structure of the closely related NiV PMD structure using the SeV, MeV or MuV PMD tetramers as starting models failed: the NiV PMD structure was eventually determined using an automated pipeline that generated search models from a set of comparative models of NiV PMD produced by *Rosetta* (Bruhn *et al.*, 2014). Failure to solve the structure of MeV and NiV PMD using the structure of PMD tetramers from closely related viruses stems from the fact that these tetramers differ in the relative orientations of their chains and hence have different superhelical parameters.

In the same vein, NiV PMD crystals showed strong off-origin peaks in self-Patterson maps, a situation reminiscent of that encountered here for both MeV PMD and PMD-Ctrunc. These off-origin peaks result from intrahelical vectors of long helices all oriented in the same direction and organized in a coiled-coil structure. The presence of these peaks underscores the inherent difficulty in solving the structure of coiled coils.

4.4. Coiled coils are less predictable than previously thought

The idealized structure of the coiled coil has been parameterized by Crick (see Lupas & Gruber, 2005 and references therein). In the structure of coiled coils, the values for pitch and crossing angle follow directly from the degree of distortion necessary to reach a periodically recurring position for the core residues. The strong heptad periodicity of coiled coils and the clear and simple parameterization of their structures have made possible a large number of computational approaches to their analysis. Their fold is probably better understood than that of any other protein. As such, their structure is thought to be predicted with confidence from a set of parametric equations. A corollary of this assumption is that the amino-acid sequence precisely dictates the coiled-coil parameters.

In striking contrast to this assumption, we here show that the same protein sequence can give rise to quite different coiled coils, differing in their inner bundle packing interactions and thus resulting in different superhelical parameters. Notably, some MeV PMD structures are almost as dissimilar from each other as from the SeV PMD structure (see Table 3), illustrating well that the amino-acid sequence is not the only determinant of the coiled-coil parameters.

The present results therefore show that coiled-coil structures can exhibit a certain degree of freedom in their twist and in the way that the single constituent chains are arranged. These differences are likely to arise from different crystallization conditions (pH, salts, precipitants *etc.*) and/or from different steric and mechanical constraints resulting from subtle differences in the chain lengths and their flexibility.

4.5. Functional implications for transcription and replication

The crystal structures of paramyxovirus PMDs solved to date have unveiled a tetrameric organization, although the organization of MuV PMD into two sets of helices with opposite orientation suggests that the minimal functional unit may be a dimer as in the case of *Rhabdovirus* P (Ivanov *et al.*, 2010; Ding *et al.*, 2006). The conservation of an oligomeric state would support a 'cartwheeling' mechanism (Curran & Kolakofsky, 1999; Kolakofsky *et al.*, 2004) whereby the N–P interaction needs to be dynamically made and broken to allow the polymerase complex to progress onto the nucleocapsid template, as opposite to a 'jumping mechanism' (Leyrat *et al.*, 2010) in which the P protein would be permanently bound to the template and the L protein would jump from one P molecule to another.

The biochemical and structural data presented here indicate that MeV PMD exists in a dynamic equilibrium between two tetramers differing in the degree of compaction. It is tempting to speculate that the different PMD tetramers observed in solution might reflect possible different functional forms of P: indeed, in infected cells the P protein forms various complexes, including L–P, N^o–P and N^o–P–L (Bourhis *et al.*, 2006; Bourhis & Longhi, 2007; Habchi & Longhi, 2012; Longhi, 2009, 2011). It is conceivable that in the various complexes the P protein may adopt different conformations leading to different extents of compaction.

Although the L-binding site has not yet been mapped within the MeV P protein, by analogy with SeV (Bowman *et*

al., 1999) it might be located in the C-terminal region of PMD. Indeed, a basic patch involved in binding to L in SeV (Tarbouriech, Curran, Ruigrok *et al.*, 2000) is also found in MeV PMD (see Fig. 3*d*). Taking into consideration the fact that this putative L-binding site is proximal to the C-terminal disordered region of PMD, and that this region may display different extents of disorder (as illustrated here through the comparison of three PMD crystal structures), it is tempting to speculate that disorder-to-order transitions could result in P forms differing in their ability to recruit and form a stable complex with L. The flexibility and malleability of PMD might be the basis for the ability of P to form different complexes critical for transcription and replication, with conformational changes possibly dictating the ability to form a transcriptase *versus* a replicase complex. Mutational studies, which are presently in progress in our laboratory, are expected to provide definite answers as to the functional role of P oligomerization and PMD flexibility.

We wish to thank Jean-Marie Bourhis (previously within the AFMB laboratory and presently within the UVHI laboratory, Grenoble) for technical help with the cloning and purification of MeV PMD. We also wish to thank Silvia Spinelli, Nicolas Foos and Miguel Lombardia-Ortiz (AFMB) for their help in data collection and analysis, and Gerlind Sulzenbacher (AFMB) for efficiently managing the AFMB BAG. We gratefully acknowledge Pierre Legrand (Proxima 1, Soleil), Philippe Carpentier (ID29, ESRF), and Petra Pernot (BM29, ESRF) for their help in data collection, and the Soleil and ESRF synchrotrons for beamtime allocation. Finally, we thank Christophe Flaudrops from the mass-spectrometry platform of the IFR48 of Marseille for mass-spectrometric analyses. This work was carried out with the financial support of the Agence Nationale de la Recherche, specific programs 'Microbiologie et Immunologie' (ANR-05-MIIM-035-02) and 'Physico-Chimie du Vivant' (ANR-08-PCVI-0020-01) to SL. It was also supported by the French Infrastructure for Integrated Structural Biology (FRISBI) (ANR-10-INSB-05-01). DB is supported by a joint doctoral fellowship from the Direction Générale de l'Armement (DGA) and the CNRS, and JE is supported by a post-doctoral fellowship from the Fondation pour la Recherche Médicale (FRM). The funders had no role in study design, data collection and analysis, decision to publish or preparation of the manuscript.

References

Adams, P. D. *et al.* (2010). *Acta Cryst.* D**66**, 213–221.
Albertini, A. A. V., Schoehn, G. & Ruigrok, R. W. (2005). *Virologie*, **9**, 83–92.
Alva, V., Syamala Devi, D. P. & Sowdhamini, R. (2008). *Protein Pept. Lett.* **15**, 33–38.
Baker, N. A., Sept, D., Joseph, S., Holst, M. J. & McCammon, J. A. (2001). *Proc. Natl Acad. Sci. USA*, **98**, 10037–10041.
Blocquel, D., Beltrandi, M., Erales, J., Barbier, P. & Longhi, S. (2013). *Virology*, **446**, 162–172.
Blocquel, D., Bourhis, J.-M., Éléouët, J.-F., Gerlier, D., Habchi, J., Jamin, M., Longhi, S. & Yabukarski, F. (2012). *Virologie*, **16**, 225–257.
Bourhis, J.-M., Canard, B. & Longhi, S. (2006). *Virology*, **344**, 94–110.
Bourhis, J.-M., Johansson, K., Receveur-Bréchot, V., Oldfield, C. J., Dunker, K. A., Canard, B. & Longhi, S. (2004). *Virus Res.* **99**, 157–167.
Bourhis, J.-M. & Longhi, S. (2007). *Measles Virus Nucleoprotein*, edited by S. Longhi, pp. 1–35. Hauppage: Nova Publishers Inc.
Bowman, M. C., Smallwood, S. & Moyer, S. A. (1999). *J. Virol.* **73**, 6474–6483.
Bruhn, J. F., Barnett, K. C., Bibby, J., Thomas, J. M. H., Keegan, R. M., Rigden, D. J., Bornholdt, Z. A. & Saphire, E. O. (2014). *J. Virol.* **88**, 758–762.
Bullough, P. A., Hughson, F. M., Skehel, J. J. & Wiley, D. C. (1994). *Nature (London)*, **371**, 37–43.
Burkhard, P., Stetefeld, J. & Strelkov, S. V. (2001). *Trends Cell Biol.* **11**, 82–88.
Chen, V. B., Arendall, W. B., Headd, J. J., Keedy, D. A., Immormino, R. M., Kapral, G. J., Murray, L. W., Richardson, J. S. & Richardson, D. C. (2010). *Acta Cryst.* D**66**, 12–21.
Communie, G., Crépin, T., Maurin, D., Jensen, M. R., Blackledge, M. & Ruigrok, R. W. (2013). *J. Virol.* **87**, 7166–7169.
Cox, R., Green, T. J., Purushotham, S., Deivanayagam, C., Bedwell, G. J., Prevelige, P. E. & Luo, M. (2013). *J. Virol.* **87**, 7558–7568.
Curran, J. & Kolakofsky, D. (1999). *Adv. Virus Res.* **54**, 403–422.
DeLano, W. L. (2002). *PyMOL*. http://www.pymol.org.
Delaunay, B. (1934). *Izv. Akad. Nauk SSSR Otdel. Mat. Est. Nauk*, **7**, 793–800.
Ding, H., Green, T. J., Lu, S. & Luo, M. (2006). *J. Virol.* **80**, 2808–2814.
Doublié, S. (1997). *Methods Enzymol.* **276**, 523–530.
Emsley, P. & Cowtan, K. (2004). *Acta Cryst.* D**60**, 2126–2132.
Franke, D. & Svergun, D. I. (2009). *J. Appl. Cryst.* **42**, 342–346.
Gely, S., Lowry, D. F., Bernard, C., Jensen, M. R., Blackledge, M., Costanzo, S., Bourhis, J.-M., Darbon, H., Daughdrill, G. & Longhi, S. (2010). *J. Mol. Recognit.* **23**, 435–447.
Habchi, J. & Longhi, S. (2012). *Mol. Biosyst.* **8**, 69–81.
Habchi, J., Mamelli, L., Darbon, H. & Longhi, S. (2010). *PLoS One*, **5**, e11684.
Huber, M., Cattaneo, R., Spielhofer, P., Örvell, C., Norrby, E., Messerli, M., Perriard, J.-C. & Billeter, M. A. (1991). *Virology*, **185**, 299–308.
Ivanov, I., Crépin, T., Jamin, M. & Ruigrok, R. W. (2010). *J. Virol.* **84**, 3707–3710.
Johansson, K., Bourhis, J.-M., Campanacci, V., Cambillau, C., Canard, B. & Longhi, S. (2003). *J. Biol. Chem.* **278**, 44567–44573.
Kabsch, W. (2010). *Acta Cryst.* D**66**, 125–132.
Karlin, D., Ferron, F., Canard, B. & Longhi, S. (2003). *J. Gen. Virol.* **84**, 3239–3252.
Karlin, D., Longhi, S. & Canard, B. (2002). *Virology*, **302**, 420–432.
Karlin, D., Longhi, S., Receveur, V. & Canard, B. (2002). *Virology*, **296**, 251–262.
Kolakofsky, D., Le Mercier, P., Iseni, F. & Garcin, D. (2004). *Virology*, **318**, 463–473.
Konarev, P. V., Volkov, V. V., Sokolova, A. V., Koch, M. H. J. & Svergun, D. I. (2003). *J. Appl. Cryst.* **36**, 1277–1282.
Lamb, R. A. & Parks, G. D. (2007). *Fields Virology*, edited by D. M. Knipe & P. M. Howley, pp. 1450–1497. Philadelphia: Lippincott Williams & Wilkins.
Lau, S. Y. M., Taneja, A. K. & Hodges, R. S. (1984). *J. Biol. Chem.* **259**, 13253–13261.
Leyrat, C., Gérard, F. C., de Almeida Ribeiro, E. Jr, Ivanov, I., Ruigrok, R. W. & Jamin, M. (2010). *Protein Pept. Lett.* **17**, 979–987.
Llorente, M. T., García-Barreno, B., Calero, M., Camafeita, E., López, J. A., Longhi, S., Ferrón, F., Varela, P. F. & Melero, J. A. (2006). *J. Gen. Virol.* **87**, 159–169.
Llorente, M. T., Taylor, I. A., López-Viñas, E., Gomez-Puertas, P., Calder, L. J., García-Barreno, B. & Melero, J. A. (2008). *Proteins*, **72**, 946–958.
Longhi, S. (2009). *Curr. Top. Microbiol. Immunol.* **329**, 103–128.
Longhi, S. (2011). *Negative Strand RNA Virus*, edited by M. Luo, pp. 95–125. Singapore: World Scientific Publishing.

Longhi, S., Receveur-Bréchot, V., Karlin, D., Johansson, K., Darbon, H., Bhella, D., Yeo, R., Finet, S. & Canard, B. (2003). *J. Biol. Chem.* **278**, 18638–18648.
Lupas, A. (1996). *Trends Biochem. Sci.* **21**, 375–382.
Lupas, A. N. & Gruber, M. (2005). *Adv. Protein Chem.* **70**, 37–78.
Meng, E. C., Pettersen, E. F., Couch, G. S., Huang, C. C. & Ferrin, T. E. (2006). *BMC Bioinformatics*, **7**, 339.
Pettersen, E. F., Goddard, T. D., Huang, C. C., Couch, G. S., Greenblatt, D. M., Meng, E. C. & Ferrin, T. E. (2004). *J. Comput. Chem.* **25**, 1605–1612.
Rahaman, A., Srinivasan, N., Shamala, N. & Shaila, M. S. (2004). *J. Biol. Chem.* **279**, 23606–23614.
Roux, L. (2005). *Virologie*, **9**, 19–34.
Spehner, D., Drillien, R. & Howley, P. M. (1997). *Virology*, **232**, 260–268.
Strelkov, S. V. & Burkhard, P. (2002). *J. Struct. Biol.* **137**, 54–64.
Sulzenbacher, G. *et al.* (2002). *Acta Cryst.* D**58**, 2109–2115.
Tarbouriech, N., Curran, J., Ebel, C., Ruigrok, R. W. & Burmeister, W. P. (2000). *Virology*, **266**, 99–109.
Tarbouriech, N., Curran, J., Ruigrok, R. W. & Burmeister, W. P. (2000). *Nature Struct. Biol.* **7**, 777–781.
Uversky, V. N. (2002). *Eur. J. Biochem.* **269**, 2–12.
Volkov, V. V. & Svergun, D. I. (2003). *J. Appl. Cryst.* **36**, 860–864.
Walshaw, J. & Woolfson, D. N. (2001). *J. Mol. Biol.* **307**, 1427–1450.
Whitmore, L. & Wallace, B. A. (2004). *Nucleic Acids Res.* **32**, W668–W673.
Whitmore, L. & Wallace, B. A. (2008). *Biopolymers*, **89**, 392–400.
Wilkins, D. K., Grimshaw, S. B., Receveur, V., Dobson, C. M., Jones, J. A. & Smith, L. J. (1999). *Biochemistry*, **38**, 16424–16431.